Pergamon

Int. J. Heat Mass Transfer. Vol. 37, No. 11, pp. 1657–1671, 1994

0017–9310/94 $7.00+0.00

0017–9310(93)E0095–X

Time-varying heat transfer from partially insulated basements

MONCEF KRARTI

Joint Center for Energy Management, CEAE Department, University of Colorado, Boulder, CO 80309-0428, U.S.A.

(*Received* 11 *February* 1993 *and in final form* 17 *November* 1993)

Abstract—The Interzone Temperature Profile Estimation (or ITPE) technique is applied to determine the steady-periodic temperature distribution within earth in contact with a partially insulated rectangular basement. A water table is assumed to exist at a given depth below the soil surface. The solution derived addresses all the common insulation configurations for basements and crawl spaces. The effect of basement depth and of partial insulation length and U-value on the mean, amplitude, and phase lag of total heat loss from the basement floor and walls is investigated through a parametric analysis.

1. INTRODUCTION

WITH THE increasing emphasis on energy conservation, basements and crawlspaces are becoming major contributors to the energy load of residential buildings. Indeed, for a typical house built before the 1970s, the basement heat losses account for as little as 10% of total envelope loads [1]. Today, the heating load related to an uninsulated but conditioned basement can represent more than 60% of the total envelope load of an energy-efficient home [2].

To reduce heat transfer from basements and crawlspaces, several insulation configurations are used. A commonly recommended configuration is to cover the upper section of the basement wall with insulation while keeping the remaining basement envelope uninsulated. This partial insulation configuration is often more cost-effective than a full insulation configuration. However, the optimal length and R-value for partial insulation may depend on several factors such as basement size and soil thermal properties.

In order to properly evaluate the optimum partial insulation length or generally the optimum insulation configuration for a basement, it is necessary that a flexible but accurate tool, for calculation of basement heat loss/gain, be available to designers and engineers. This tool should be able to predict heat fluxes for a continuous set of basement geometries, soil thermal properties, indoor and outdoor temperature variations, and common insulation configurations.

Over a dozen methods for calculating heat transfer from basements and crawlspaces are now available. Most of these methods have been reviewed by Sterling and Meixel [3] and/or by Claridge [4]. Virtually all of the existing basement heat loss calculation methods are based on numerical techniques such as finite differences or finite elements. Among the well documented and influential methods for ground heat transfer calculation are those by Mitalas [5], Shipp [6], and Shen [7]. Mitalas compiled tables of shape factors to accommodate a comprehensive set of basement and slab-on-grade floor insulation configurations. These shape factors are computed from a two-dimensional finite element program complemented with empirical data to include corner effects. The Mitalas shape factors are given for a discrete set of insulation and soil thermal properties values. The Shipp method [6] employs the Pantakar and Spalding implicit finite difference technique to calculate heat transfer from basements and crawlspaces. Shipp's approach can model several deep and shallow basement insulation configurations and permits variable soil properties. Shipp used a time step of one day, and in some cases larger time steps were assumed to calculate heat fluxes from the basement envelope. Shen and Ramsey [7] developed a two-dimensional solution to the heat transfer problem around a basement. This solution is based on the same Pantakar–Spalding approach used by Shipp. To reduce storage requirements, Shen *et al.* complemented the numerical method with the Fourier series technique [8]. Recently, Shen *et al.* extended their model to include most of the common basement insulation configurations [9]. The data generated from the finite difference model are restricted to certain insulation lengths and R-values.

While other detailed models exist, the three methods described above provide a representation of common approaches in the study of heat transfer between basements and ground. Because, they are based on numerical techniques, the existing methods use relatively large time steps. In addition, most assume constant interior temperature. Hence they fail to account for hourly effects on ground-coupled heat transfer of temperature fluctuations due to thermostat setting, solar gain, and/or lighting schedule. These effects can be significant. Using a frequency response analysis,

NOMENCLATURE

a	basement half width [m]
A_n, B_n, C_n, D_n	general term in a Fourier series expansion
b	water table depth [m]
c	basement depth [m]
d	floor insulation location from the center of the basement [m]
e	wall insulation length from soil surface [m]
f, g	functions of one of the space coordinates [K]
f_n, g_n	Fourier coefficients
H	ratio, h/k_s [m^{-1}]
h	overall heat transfer conductance [W m^{-2} K^{-1}]
k_s	soil thermal conductivity [W m^{-1} K^{-1}]
L	distance from building center to a boundary where soil temperature is undisturbed [m]
Q	total heat loss [W m^{-1}]
$\tilde{Q}$	complex amplitude of total heat loss $(1+i)$ [W m^{-1}]
t	time [s]
T	temperature [K]
$\tilde{T}$	complex temperature amplitude, $(1+i)$ [K]
T_i	building indoor air temperature [K]
T_s	soil surface temperature [K]
T_u	undisturbed soil temperature [K]
T_w	water table temperature [K]
x,y	space coordinates [m].

Greek symbols

α, β, γ	coefficients defined in equations (6), (8), (11), and (13)
ζ_n, χ_n, ν_n, μ_n	eigenvalues [m^{-1}]
κ_s	soil thermal diffusivity [m^2 s^{-1}]
ϕ	phase lag [rad]
ω	angular frequency [rad s^{-1}].

Subscripts

a	amplitude
f	floor
fm	middle of the floor
fe	edge of the floor
m	annual mean
s	steady-state or mean
t	transient amplitude
wa	wall
wl	lower part of the wall
wt	top part of the wall
I	zone (I)
II	zone (II)
III	zone (III).

Kusuda *et al.* [10] found that diurnal fluctuations in indoor temperature have a large impact on the slab-on-grade floor heat loss/gain.

In this paper, a two-dimensional analytical solution to the heat conduction equation is developed for partially insulated basements under steady-periodic conditions. The interior temperature of the basement is allowed to change with time. A water table at finite depth from the soil surface is considered. The solution presented is the first analytical solution for basements capable of analyzing the effects of partial insulation and water table depth on foundation heat transfer. The solution presented in this paper is based on the Interzone Temperature Profile Estimation (ITPE) technique. This technique has been successfully applied to solve time-varying two-dimensional and three-dimensional heat transfer problems from uniformly insulated basements [11, 12]. This paper presents a more general time-varying two-dimensional solution that can handle a variety of basement insulation configurations including uninsulated, fully insulated, and partially insulated walls and floors.

This paper provides physical insight on how heat flows from basements to ground and shows the effect of partial insulation on the soil temperature field and on the total amount of heat flowing from basement surfaces in contact with earth. In Section 2, the general solution of heat time-dependent heat diffusion equation is developed. In Section 3, the soil temperature field is illustrated for several basement insulation configurations. Finally in Section 4, a parametric analysis is conducted to show the effect of the insulation length and U-value on both the basement wall and floor heat losses. Throughout this section, annual fluctuations are assumed; however, the solution developed in this paper is valid for any other period of time.

2. FORMULATION OF THE PROBLEM

The basement problem with partial insulation along the floor and the walls is modeled as shown in Fig. 1(a). Along the bounding surfaces $x = \pm L$, the soil temperature is assumed to be undisturbed by the basement. Note that the model of Fig. 1(a) does not show basement construction details such as footings and foundation walls. These foundation elements are generally made up of poured or precast concrete. Since the thermal conductivity of ground is typically similar to that of concrete, the foundation elements can be considered as integral parts of the ground medium. The model of Fig. 1(a) provides a realistic approximation of a rectangular basement with interior insulation. When the insulation is placed on the exterior of the basement walls and/or floor, thermal bridging may occur along the concrete section of the basement envelope. However, this thermal bridging is minimal

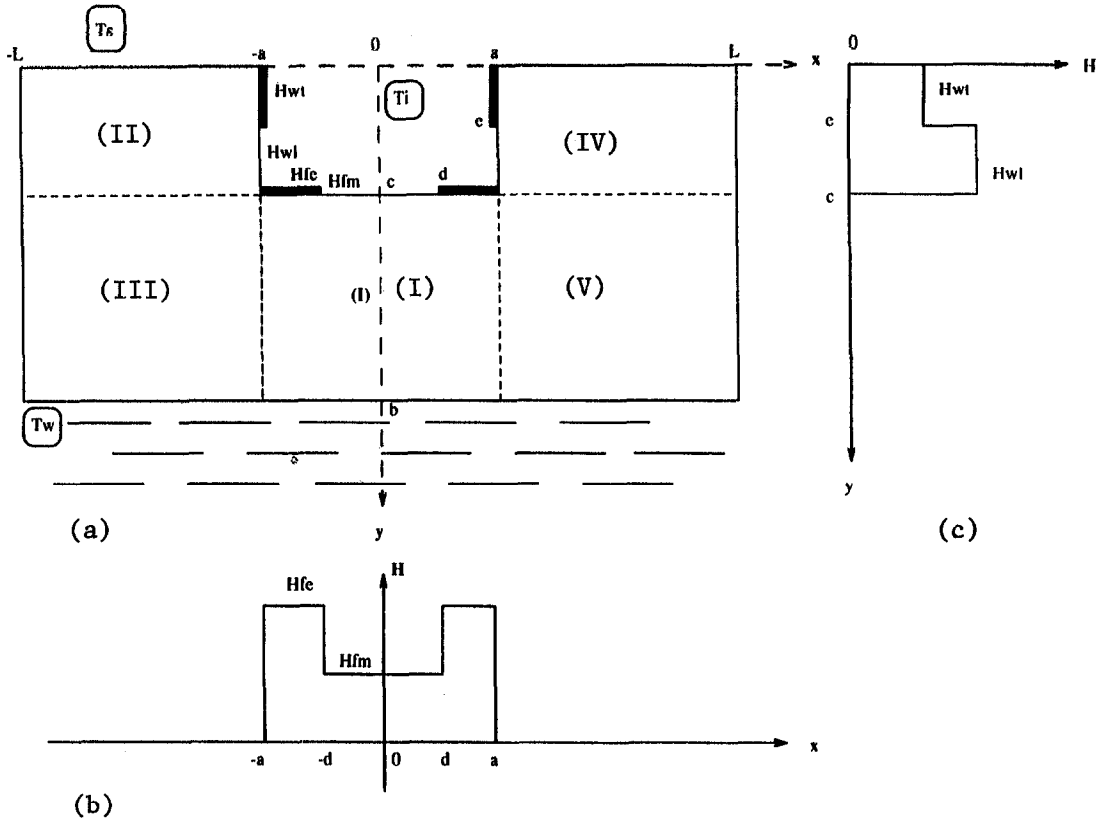

FIG. 1. (a) Rectangular basement with partial insulation, (b) floor insulation distribution, (c) wall insulation distribution.

when the above grade portion of the basement walls are insulated. Using a more elaborate model for basements that takes into account the concrete walls, it was found that interior and exterior insulation placement provide virtually identical thermal performance [2].

When all temperatures vary periodically with time at angular frequency ω, the temperature distribution $T(x,y,t)$, around the rectangular basement, is subject to the heat diffusion equation:

$$\frac{\partial^2 T}{\partial x^2}+\frac{\partial^2 T}{\partial y^2}=\frac{1}{\kappa_s}\frac{\partial T}{\partial t} \tag{1}$$

with

$$k_s\frac{\partial T}{\partial y}=h_f(x)(T_i-T) \text{ and } T_i=T_{im}+T_{ia}\cos(\omega t+\phi_i)$$

$$\text{for } y=c \text{ and } |x|<a$$

$$k_s\frac{\partial T}{\partial x}=h_{wa}(y)(T-T_i) \quad \text{for } y<c \text{ and } |x|=a$$

$$T=T_{sm}+T_{sa}\cos(\omega t+\phi_s) \quad \text{for } y=0 \text{ and } |x|>a$$

$$T=T_u(y,t) \quad \text{for } |x|=L$$

$$T=T_{ws}+T_{wa}\cos(\omega t+\phi_w) \quad \text{for } y=b.$$

Note that the temperature of air at the basement interior, soil surface, and water table are characterized by a mean, an amplitude, and a phase lag. Even though the above equation applies to any angular frequency, the examples and analyses presented throughout this section will assume annual frequency (i.e. $\omega = 1.992\times10^{-7}$ rad s^{-1}).

The conductance values $h_f(x)$ and $h_{wa}(y)$ account for the convective film coefficient at the inner surface of the slab, the insulation U-value, and the foundation material conductance, for floor and walls, respectively. The values of $h_f(x)$ and $h_{wa}(y)$ vary along the foundation surfaces. In this paper, stepped functions are assumed for both h_f and h_{wa} as illustrated in Fig. 1(b) and Fig. 1(c).

At locations far from the basement ($x = \pm L$), the soil temperature, T_u, is undisturbed and is a function of only depth y and time t.

In steady-periodic conditions, the solution $T(x,y,t)$ of equation (1), can be obtained from a complex temperature $\tilde{T}(x, y)$ solution of the following Helmholtz equation:

$$\frac{\partial^2 \tilde{T}}{\partial x^2}+\frac{\partial^2 \tilde{T}}{\partial y^2}=\delta^2\tilde{T} \tag{2}$$

with

$$\delta=\sqrt{(i\omega/\kappa_s)}.$$

The boundary conditions of equation (1) become:

$$\frac{\partial \tilde{T}}{\partial y} = H_f(x)(\tilde{T}_i - \tilde{T}) \quad \text{for } y = c \text{ and } |x| < a$$

$$k_s \frac{\partial \tilde{T}}{\partial x} = H_{wa}(y)(\tilde{T} - \tilde{T}_i) \quad \text{for } y < c \text{ and } |x| = a$$

$$\tilde{T} = \tilde{T}_s \quad \text{for } y = 0 \text{ and } |x| > a$$

$$\tilde{T} = \tilde{T}_u \quad \text{for } |x| = L$$

$$\tilde{T} = \tilde{T}_w \quad \text{for } y = b$$

where $H_f(x) = h_f(x)/k_s$ and $H_{wa}(y) = h_{wa}(y)/k_s$. Physically, the value of $1/H_f$ represents the equivalent thickness of a soil layer that would have a U-value equal to h_f. Similar interpretation can be given to the value of $1/H_{wa}$.

In the formulation of equation (2) the water table temperature $\tilde{T}_w$ can be set to zero without loss of generalization. The water table temperature will become the origin of temperature.

In order to solve the Helmholtz equation (2), the Interzone Temperature Profile Estimation (ITPE) technique will be used. As indicated in Fig. 1(a), the ground can be divided into five zones imposed by the basement geometry. Since the basement configuration has an axial symmetry around $x = 0$, the determination of the temperature variation in zones (I), (II), and (III) will be sufficient. Furthermore, the temperature profiles at the surfaces $x = -a$ and $y = c$ are functions of y and x, respectively:

$$\tilde{T}(-a, y) = f(y) \quad c < y < b$$

and

$$\tilde{T}(x, c) = g(x) \quad -L < x < -a.$$

Using the separation of variables technique, the solution in zone (I) is

$$\tilde{T}_I(x, y) = \frac{2}{(b-c)} \sum_{n=1}^{+\infty} f_n \sin \nu_n (y-c) \frac{\cosh \nu'_n x}{\cosh \nu'_n a} + \frac{2}{a} \sum_{n=1}^{+\infty} C_n \cos \mu_n x \frac{\sinh \mu'_n (b-y)}{\sinh \mu'_n (b-c)}. \quad (3)$$

In zone (III), the solution is given by

$$\tilde{T}_{III}(x, y) = \frac{2}{(L-a)} \sum_{n=1}^{+\infty} g_n \sin \chi_n (x+a) \frac{\sinh \chi'_n (b-y)}{\sinh \chi'_n (b-c)} + \frac{2}{(b-c)} \sum_{n=1}^{+\infty} f_n \sin \nu_n (y-c) \frac{\sinh \nu'_n (x+L)}{\sinh \nu'_n (L-a)} + \frac{2}{(b-c)} T_s \sum_{n=1}^{+\infty} \frac{(b-c)/b}{\nu_n} \sin \nu_n (y-c) \frac{\sinh \nu'_n (x+a)}{\sinh \nu'_n (a-L)}. \quad (4)$$

The expression for the temperature in zone (II) takes a more complex form:

$$\tilde{T}_{II} = \frac{2}{(L-a)} T_s \sum_{n=1}^{+\infty} \frac{[(-1)^n - 1]}{\chi_n} \times \sin \chi_n (x+a) \frac{\sinh \chi'_n (c-y)}{\sinh \chi'_n c} + \frac{2}{(L-a)} \sum_{n=1}^{+\infty} g_n \sin \chi_n (x+a) \times \frac{\sinh \chi'_n y}{\sinh \chi'_n c} + \frac{2}{c} T_s \sum_{n=1}^{+\infty} \frac{[1-(-1)^n (b-c)/b]}{\zeta_n} \times \sin \zeta_n y \frac{\sinh \zeta'_n (x+a)}{\sinh \zeta'_n (a-L)} + \frac{2}{c} \sum_{n=1}^{+\infty} D_n \sin \zeta_n y \frac{\sinh \zeta'_n (x+L)}{\sinh \zeta'_n (L-a)} \quad (5)$$

where

$$\nu_n = \frac{n\pi}{(b-c)}; \quad \nu'_n = \sqrt{(\nu_n^2 + \delta^2)}$$

$$\chi_n = \frac{n\pi}{(L-a)}; \quad \chi'_n = \sqrt{(\chi_n^2 + \delta^2)}$$

$$\zeta_n = \frac{n\pi}{c}; \quad \zeta'_n = \sqrt{(\zeta_n^2 + \delta^2)}$$

$$\mu_n = \frac{(2n-1)\pi}{2a}; \quad \mu'_n = \sqrt{(\mu_n^2 + \delta^2)}$$

$$f_n = \int_c^b f(y) \sin \nu_n (y-c) \mathrm{d}y$$

$$g_n = \int_{-L}^{-a} g(x) \sin \chi_n (x+a) \mathrm{d}x.$$

The Fourier coefficients f_n, g_n, C_n, and D_n defined above are determined from the required continuity of the heat flux along the surfaces $x = -a$ and $y = c$.

First, the third kind boundary condition of equation (2) at $y = c$ states that:

$$\left.\frac{\partial \tilde{T}_I}{\partial y}\right|_{y=c} = H_f(x)(\tilde{T}_I - \tilde{T}_i)$$

or, using the expression (3) for the temperature $\tilde{T}_I$:

$$\frac{2}{(b-c)} \sum_{n=1}^{+\infty} \nu_n f_n \frac{\cosh \nu'_n x}{\cosh \nu'_n a} - \frac{2}{a} \sum_{n=1}^{+\infty} \mu_n C_n \coth \mu'_n (b-c) \cos \mu_n x = H_f(x) \left(\frac{2}{a} \sum_{n=1}^{+\infty} C_n \cos \mu_n x - \tilde{T}_i \right). \quad (6)$$

Multiplying this equation by $\cos \mu_p x$ and integrating over the interval $[0, a]$ gives:

$$C_p = \alpha_p^C + \sum_{n=1}^{+\infty} \beta_{n,p}^C f_p + \sum_{n=1}^{+\infty} \gamma_{n,p}^C C_n \quad (7)$$

with

$$\alpha_p^C = \frac{(H_{fm} - H_{fe}) \sin \mu_p c - (-1)^p H_{fe} \tilde{T}_i}{\mu_p (H_{fe} + \mu'_p \coth \mu'_p (b-c))}$$

$$\beta^{C}_{n,p} = -\frac{2}{(b-c)}\frac{(-1)^p \nu_n \mu_p}{(\mu_p^2+\nu_n'^2)(H_{fe}+\mu_p'\coth\mu_p'(b-c))}$$

and

$$\gamma^{C}_{n,p} = \frac{1}{a}\frac{(H_{fe}-H_{fm})}{(H_{fe}+\mu_p'\coth\mu_p'(b-c))} \times\left\{\frac{\sin(\mu_n-\mu_p)d}{(\mu_n-\mu_p)}+\frac{\sin(\mu_n+\mu_p)d}{(\mu_n+\mu_p)}\right\}.$$

The third kind boundary condition of equation (1) at $x=-a$ can be written as follows:

$$\left.\frac{\partial\tilde{T}_{II}}{\partial x}\right|_{x=-a} = H_{wa}(y)\,(\tilde{T}_i-\tilde{T}_{II})$$

or, using the expression (5) for the temperature $\tilde{T}_{II}$:

$$\frac{2}{(L-a)}\sum_{n=1}^{+\infty}((-1)^n-1)\tilde{T}_s\frac{\sinh\chi_n'(c-y)}{\sinh\chi_n'c} + \frac{2}{(L-a)}\sum_{n=1}^{+\infty}\chi_n g_n\frac{\sinh\chi_n'y}{\sinh\chi_n'c} \times\frac{2}{c}\sum_{n=1}^{+\infty}\left[1-(-1)^n\left(1-\frac{c}{b}\right)\right]\zeta_n'\tilde{T}_s\frac{\sin\zeta_n y}{\sinh\zeta_n'(L-a)} + \frac{2}{c}\sum_{n=1}^{+\infty}\zeta_n D_n\coth\zeta_n'(L-a)\sin\zeta_n y = H_{wa}(x)\left(\tilde{T}_i-\frac{2}{c}\sum_{n=1}^{+\infty}D_n\sin\zeta_n y\right). \quad (8)$$

Multiplying this equation by $\sin\zeta_p y$ and integrating over the interval [0,c] gives a system of linear equations:

$$D_p = \alpha_p^D+\sum_{n=1}^{+\infty}\beta_{n,p}^D D_n+\sum_{n=1}^{+\infty}\gamma_{n,p}^D g_n \quad (9)$$

with

$$\alpha_p^D = \frac{1}{(H_{wl}+\zeta_p'\coth\zeta_p'(L-a))} \times\left\{\frac{(-1)^p(b-c)\tilde{T}_s}{b\sinh\zeta_p'(L-a)}-\tilde{T}_s\coth\zeta_p'(L-a) +H_{wt}\left(\frac{1-\cos\zeta_p e}{\zeta_p'}\right)\tilde{T}_i+H_{wl}\left(\frac{\cos\zeta_p e-(-1)_p}{\zeta^p}\right)\tilde{T}_i\right\}$$

$$\beta_{n,p}^D = \frac{1}{c}\frac{(H_{wl}-H_{wt})}{(H_{wl}+\zeta_p'\coth\zeta_p'(L-a))} \times\left\{\frac{\sin(\zeta_n-\zeta_p)e}{(\zeta_n-\zeta_p)}+\frac{\sin(\zeta_n+\zeta_p)e}{\zeta_n+\zeta_p}\right\}$$

and

$$\gamma_{n,p}^D = -\frac{2}{(L-a)}\frac{(-1)^p\chi_n\zeta_p}{(H_{wl}+\zeta_p'\coth\zeta_p'(L-a))(\chi_n'^2+\zeta_p^2)}.$$

For $x=-a$, flux continuity states that

$$\left.\frac{\partial\tilde{T}_I}{\partial x}\right|_{x=-a} = \left.\frac{\partial\tilde{T}_{III}}{\partial x}\right|_{x=-a}. \quad (10)$$

After a computation procedure similar to that followed for the third-boundary conditions, equation (10) leads to:

$$f_p = \alpha_p^f+\sum_{n=1}^{+\infty}\beta_{n,p}^f C_n+\sum_{n=1}^{+\infty}\gamma_{n,p}^f g_n \quad (11)$$

with

$$\alpha_p^f = \frac{2}{(L-a)}\frac{(b-c)}{b} \times\frac{\tilde{T}_s}{\nu_p\sinh\nu_p'(L-a)(\tanh\nu_p'a+\coth\nu_p'(L-a))}$$

$$\beta_{n,p}^f = -\frac{2}{a}\frac{(-1)^n\mu_n\nu_p}{(\mu_n^2+\nu_p^2)(\tanh\nu_p'a+\coth\nu_p'(L-a))}$$

$$\gamma_{n,p}^f = -\frac{2}{(L-a)} \times\frac{\nu_p\chi_n}{(\nu_p^2+\chi_n'^2)(\tanh\nu_p'a+\coth\nu_p'(L-a))}.$$

The condition of the heat flux continuity at the surface $y=c$ is expressed by:

$$\left.\frac{\partial\tilde{T}_{II}}{\partial y}\right|_{y=c} = \left.\frac{\partial\tilde{T}_{III}}{\partial y}\right|_{y=c}. \quad (12)$$

This condition yields a system of equations of the form:

$$g_p = \alpha_p^g+\sum_{n=1}^{+\infty}\beta_{n,p}^g f_n+\sum_{n=1}^{+\infty}\gamma_{n,p}^g D_n \quad (13)$$

where

$$\alpha_p^g = \frac{1}{\chi_p(\coth\chi_p'c+\coth\chi_p'(b-c))} \times\left\{\frac{-\tilde{T}_s}{\sinh\chi_p'c}+(1-c/b)(-1)^p\tilde{T}_s\coth\chi_p'c -\frac{(1-c/b)\tilde{T}_i}{\sinh\chi_p'(b-c)}\right\}$$

$$\beta_{n,p}^g = -\frac{2}{(b-c)}\frac{\nu_n\chi_p}{(\nu_n'^2+\chi_p^2)(\coth\chi_p'c+\coth\chi_p'(b-c))}$$

$$\gamma_{n,p}^g = -\frac{2}{c}\frac{(-1)^n\zeta_n\chi_p}{(\coth\chi_p'c+\coth\chi_p'(b-c))(\zeta_n'^2+\chi_p^2)}.$$

The Fourier coefficients f_p, g_p, C_n, and D_n are determined by truncating the sums in (7), (9), (11), and (13), to N terms. By doing so, a system of $4N$ equations with $4N$ unknowns ($f_1, f_2, \ldots, f_N$; $g_1, g_2, \ldots, g_N$; C_1, $C_2, \ldots, C_N$; and $D_1, D_2, \ldots, D_N$) is obtained. This system can be easily solved using standard methods (e.g. Gauss–Jordan elimination).

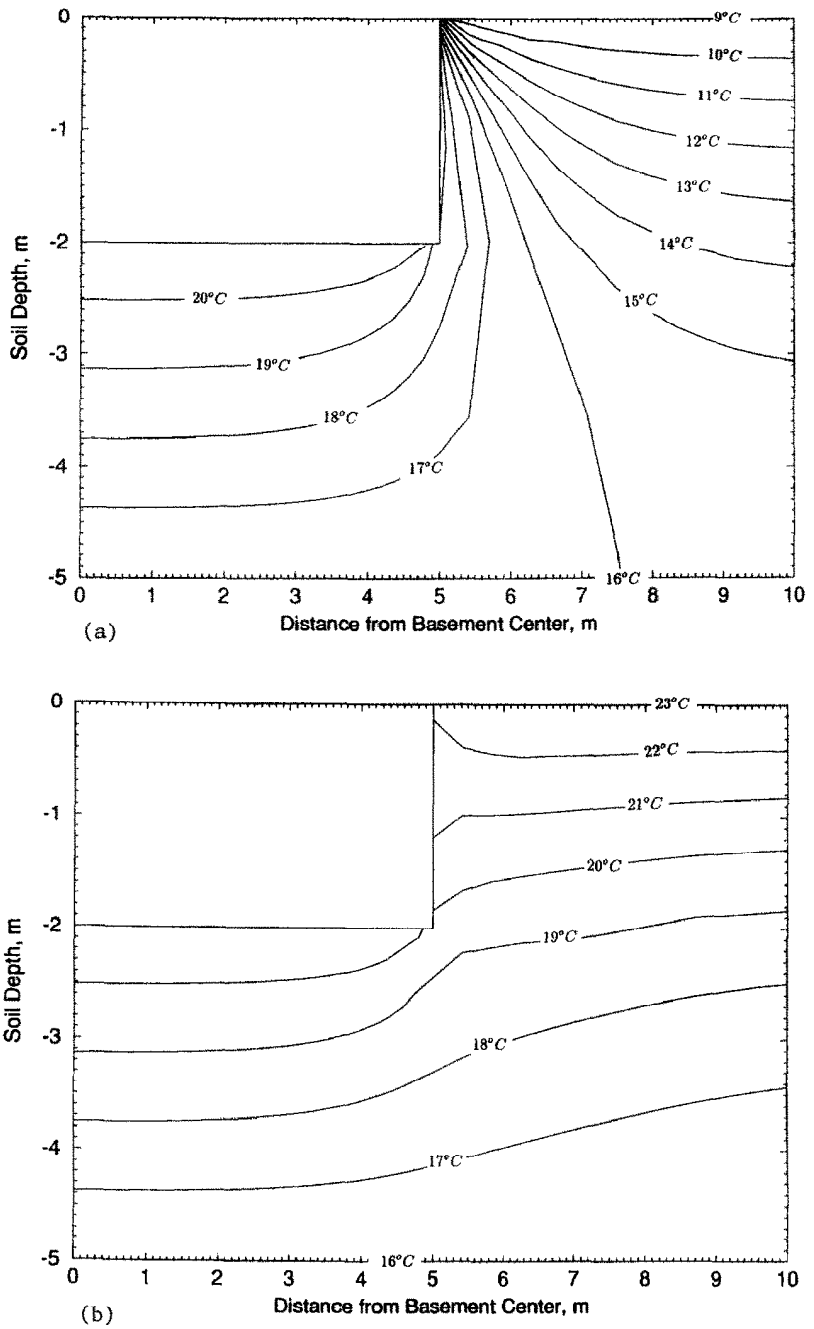

FIG. 2. Earth temperature isotherms around an uninsulated basement for (a) wintertime, (b) summertime.

3. TEMPERATURE DISTRIBUTION

Figures 2–6 show the soil temperature field around a rectangular basement on 15 January (winter) and 15 July (summer). The basement has a width of $2a = 10$ m and a depth of $c = 2$ m. The interior air temperature of the basement is kept constant at $T_i = 2°C$, while the soil surface temperature varies sinusoidally with time as $T_s(°C) = 16 - 7\cos(\omega t)$ where $\omega = 1.992 \times 10^{-7}$ rad s^{-1} is the annual angular frequency. A water table exists at a depth $b = 5$ m and has a constant temperature $T_w = 16°C$. The soil has a thermal conductivity of $k_s = 1.0$ W m^{-1}K^{-1}, and a thermal diffusivity of $\kappa_s = 6.45 \times 10^{-7}$ m^2 s^{-1}.

Five different insulation configurations are considered:

(i) Uninsulated basement, Fig. 2.
($H_{wl} = H_{wt} = H_{fm} = H_{fe} = 10$ m^{-1}.)

(ii) Basement with partial insulation over the top 1 m of the wall, Fig. 3.
($H_{wt} = 0.5$ m^{-1}; $H_{wl} = H_{fm} = H_{fe} = 10$ m^{-1}; $e = 1$ m.)

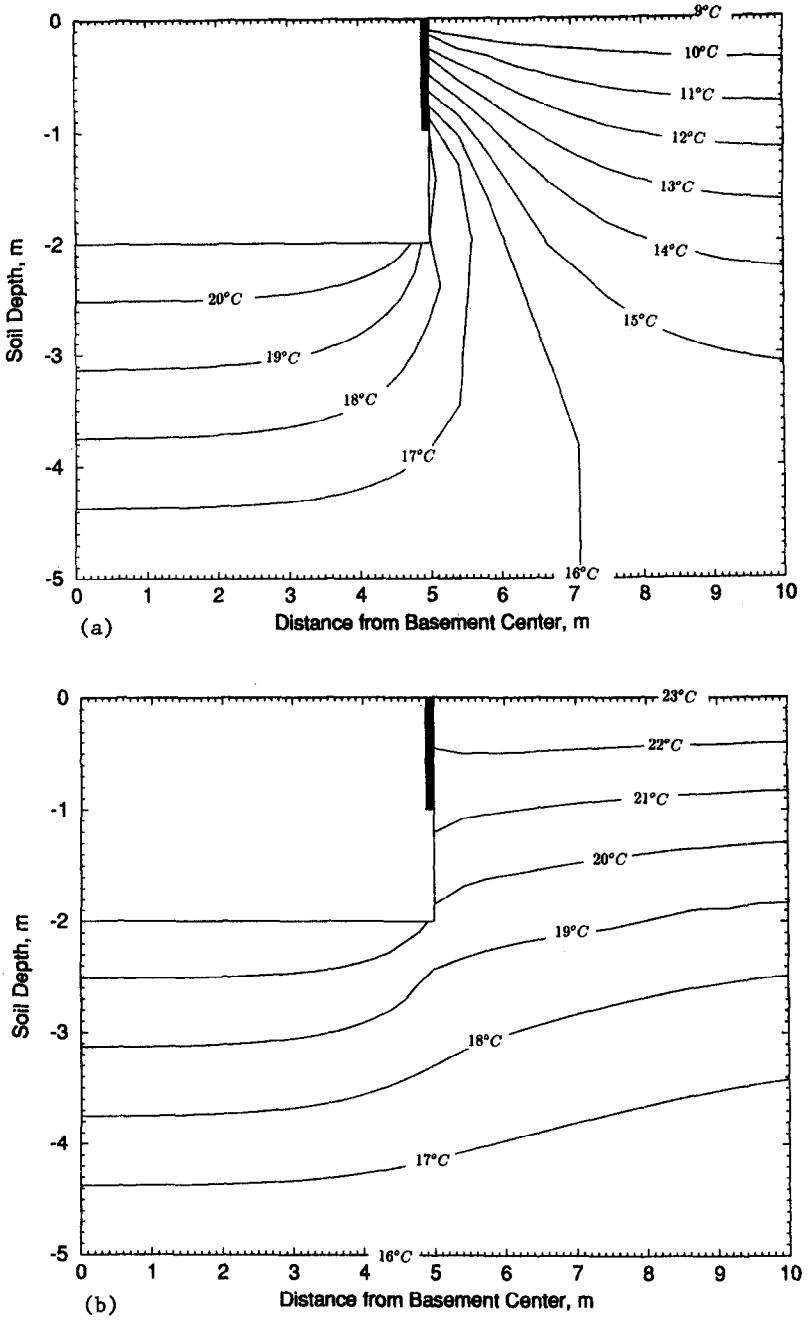

FIG. 3. Earth temperature isotherms around a basement with 1 m-long partial wall insulation for (a) wintertime, (b) summertime.

(iii) Basement with insulation over the full height of the wall, Fig. 4.
($H_{wt} = H_{wl} = 0.5\ m^{-1}$; $H_{fm} = H_{fe} = 10\ m^{-1}$.)

(iv) Basement with insulation over the full height of the wall and partial insulation along 1 m of the floor perimeter, Fig. 5.
($H_{wt} = H_{wl} = H_{fe} = 0.5\ m^{-1}$; $H_{fm} = 10\ m^{-1}$; $d = 4$ m.)

(v) Basement with uniform insulation over the walls and along the floor, Fig. 6.
($H_{wt} = H_{wl} = H_{fe} = H_{fm} = 0.5\ m^{-1}$.)

The effect of gradually adding insulation along the basement envelope on winter and summer soil temperature fields is shown in Figs. 2–6. Generally, the insulation reduces the magnitude of temperature change along the basement envelope. In the uninsulated case during wintertime (Fig. 2(a)), the temperature at the top portion of the basement wall varies abruptly from 9°C to 18°C within 0.2 m of the soil surface. This sudden change in temperature indicates a high rate of heat transfer between the ground and the upper portion of the basement walls. On the water

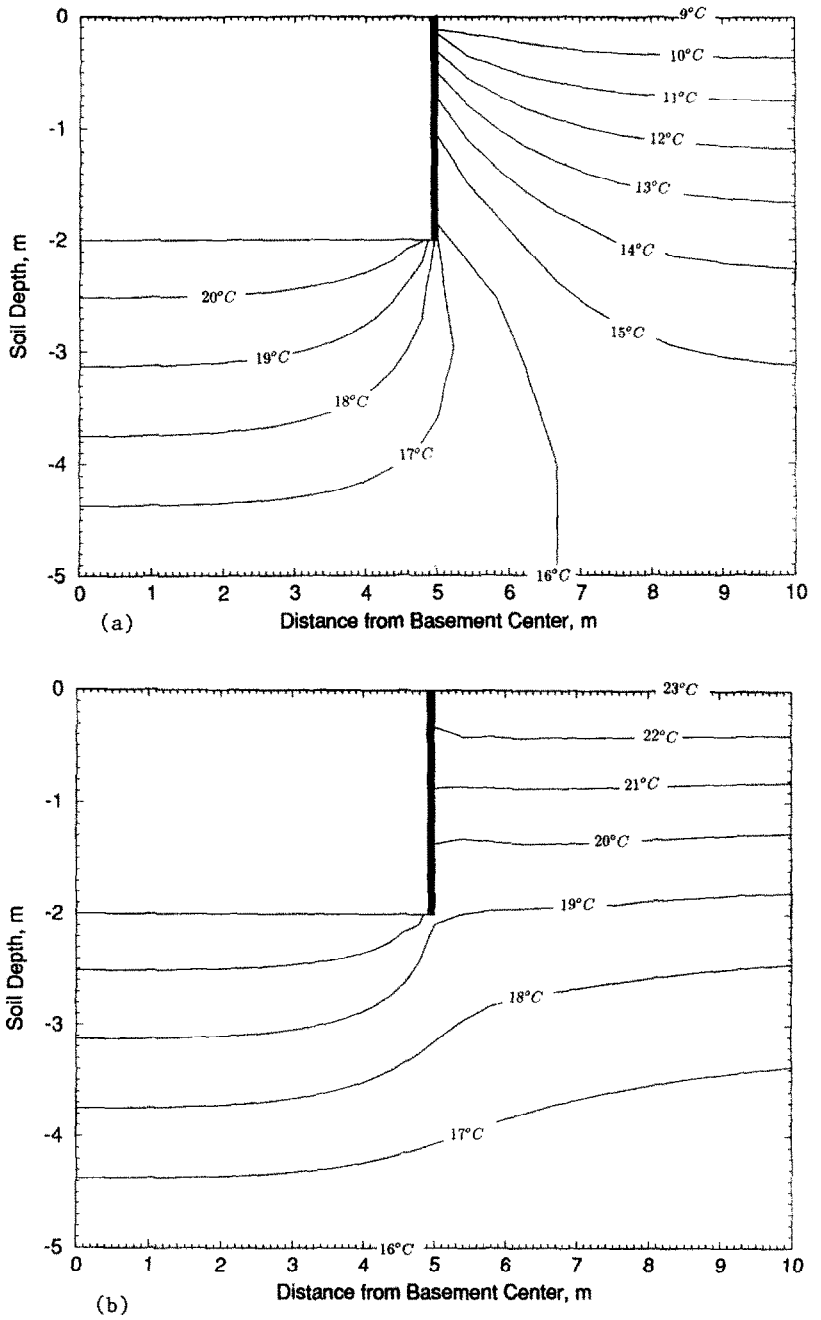

FIG. 4. Earth temperature isotherms around a basement with full wall insulation for (a) wintertime, (b) summertime.

table surface about 7.5 m from the basement center, a double point exists. This double point marks the meeting of the water table surface (kept at the temperature 16°C) and the soil isotherm of 16°C. To the left side of the double point, the water table receives heat from the basement envelope, while to the right side, the water table loses heat mostly to the soil surface. Figure 2(b) indicates that during the summer, the upper portion of the walls is warmer than the remaining basement envelope. At about mid-section of the walls, a double point appears. Above this double point, the basement walls gain heat from the warmer soil surface. Meanwhile, below the double point, the basement envelope loses heat to the colder water table surface.

When insulation is added to the upper half of the basement walls, the wintertime soil temperature decreases, especially in the vicinity of the soil surface–basement wall joint (Fig. 3(a)). In very cold climates where soil surface temperature is below freezing, the

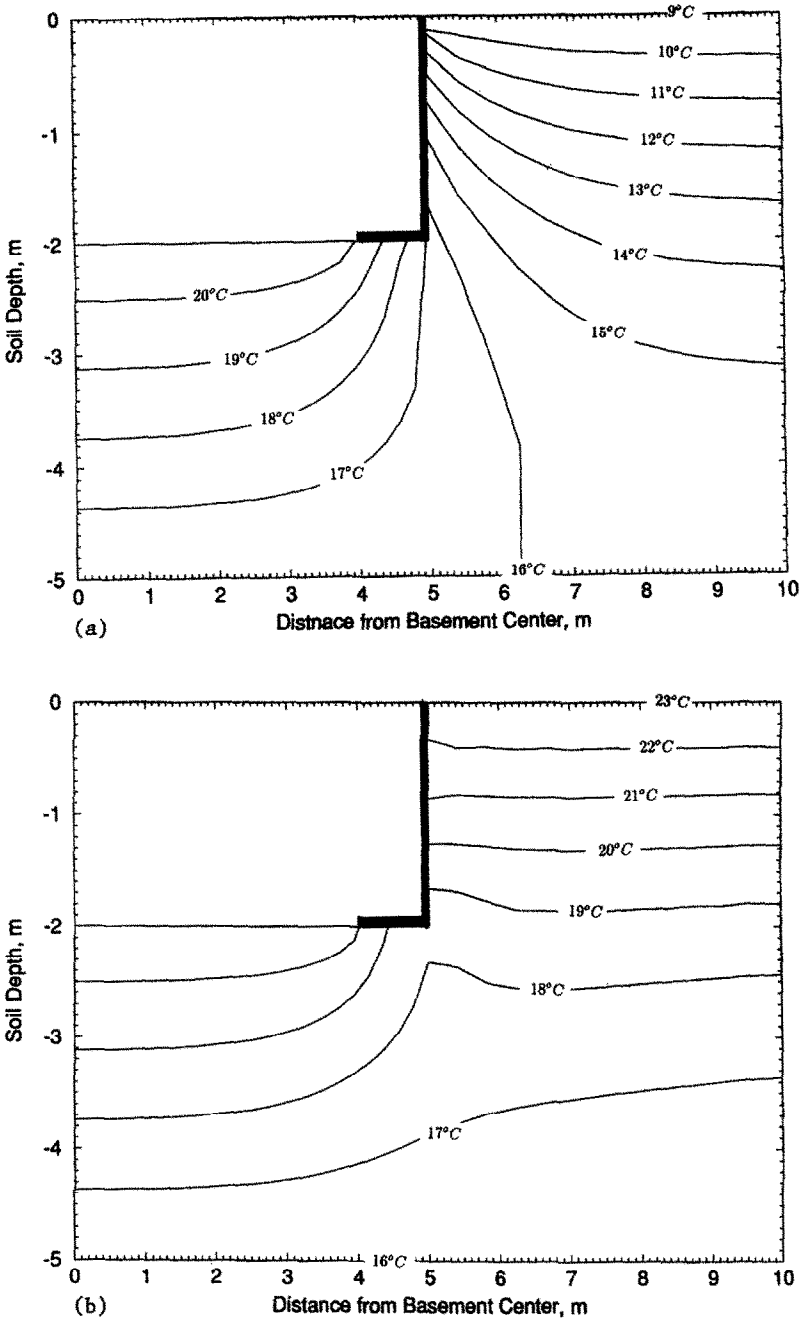

FIG. 5. Earth temperature isotherms around a basement with full wall insulation and 1-m wide floor edge insulation for (a) wintertime, (b) summertime.

foundation area affected by frost increases as insulation is added to the interior of basement walls. Figure 3(a) shows also that the temperature gradient along the upper portion of the walls is reduced implying a decrease in heat loss. In addition, it is interesting to note that the double point on the water table surface moved closer and is now about 7 m from the basement center. This new double point location indicates that the water table is thermally more affected by the soil surface than the basement envelope. The effect of wall partial insulation on the summertime soil temperature field is shown in Fig. 3(b). Except for a slight increase in the temperature of the upper portion of the basement wall, the soil temperature distribution is not affected by the partial wall insulation during summer.

As the insulation is extended to full wall height, the decrease in wintertime soil temperature continues in the vicinity of the basement walls (Fig. 4(a)). The temperature gradient and thus heat flux along the basement walls has also decreased. However, the temperature gradient at the basement floor edges has

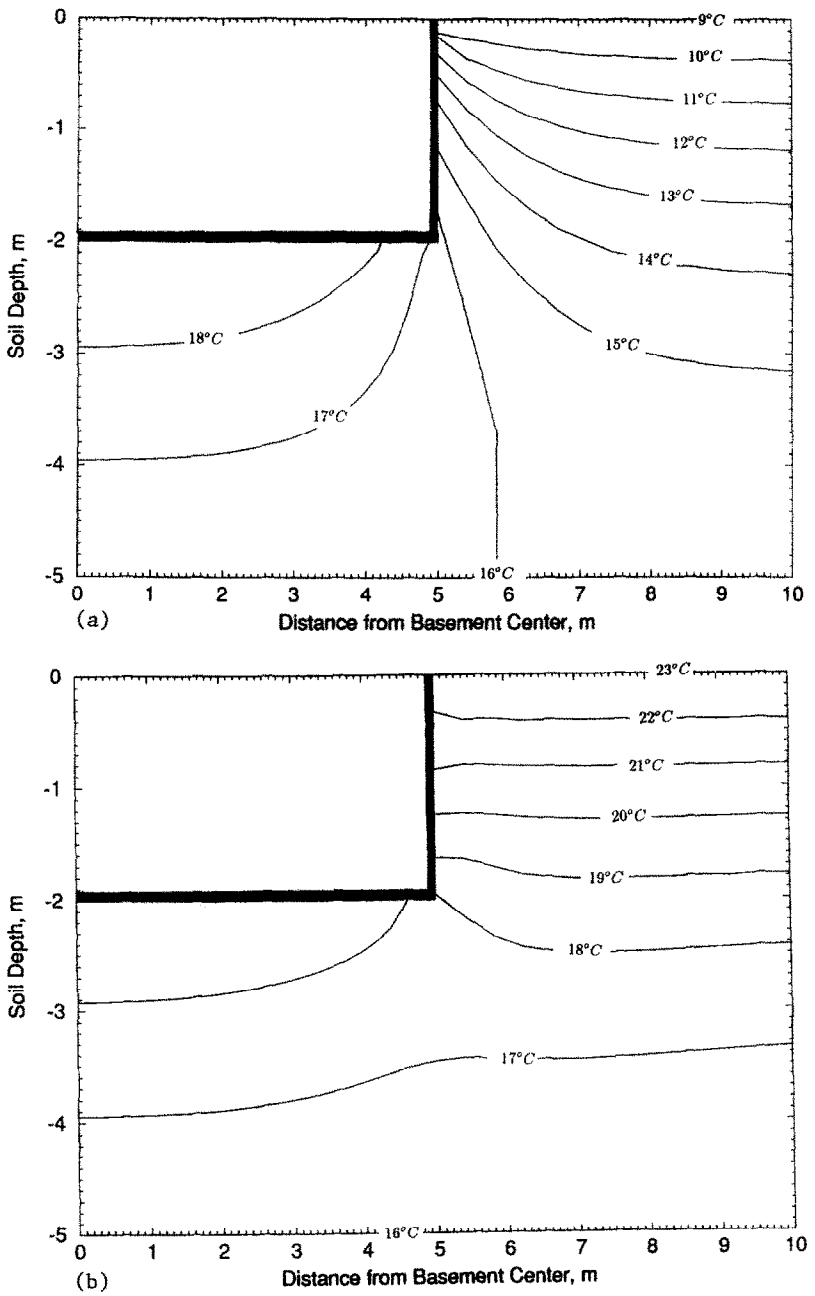

FIG. 6. Earth temperature isotherms around a basement with uniform insulation for (a) wintertime, (b) summertime.

increased as a result of the full wall insulation. The double point at the water table continues to move closer to the basement center. During the summer (Fig. 4(b)), soil temperature in the vicinity of the basement wall varies almost linearly with depth. In particular, the double point of the basement wall has moved upward indicating that the thermal interaction between soil surface and basement is reduced.

Figure 5(a) shows the wintertime soil temperature distribution when insulation is placed along the full height of the walls and along a 1 m wide strip of the floor. As expected, the temperature gradient in the vicinity of the basement floor edges is reduced. In addition, the temperature of the lower portion of the wall has increased slightly as a result of the partial floor insulation. During the summer, the temperature is reduced at the floor-wall corners as indicated in Fig. 5(b). Notice that soil temperature field beneath the basement floor center stays almost unchanged throughout the year. Indeed, the center of the basement floor interacts strongly with the water table surface which has a constant temperature.

When insulation is placed uniformly on the entire basement envelope surface, the floor temperature is

reduced during both winter and summer as illustrated in Fig. 6. The floor temperature varies between 19°C (at the center) and 17°C (at the edges) during wintertime, and between 19°C (at the center) and 18°C (at the edges) during summertime. Figure 6(a) indicates that the water table double point is now less than 6 m away from the basement center. Thus the added full floor insulation reduces the extent of water table area that receives heat from the basement.

4. TOTAL BASEMENT HEAT LOSS

The time variation of total basement heat loss $Q_f(t)$ has two parts: steady-state, $Q_{f,s}$, and transient $Q_{f,t}$:

$$Q_f(t) = Q_{f,s} + Re(Q_{f,t}\, e^{i\omega t}). \tag{14}$$

Both $Q_{f,s}$ and $Q_{f,t}$ are obtained from the complex amplitude of the total basement floor heat loss $\tilde{Q}_f$.

$$\tilde{Q}_f = 2\left\{H_{fm}\left(-T_s d + \frac{2}{a}\sum_{n=1}^{+\infty}\frac{C_n}{\mu_n}\sin\mu_n d\right)\right.$$

$$\left. -H_{fe}\left((a-d)T_s + \frac{2}{a}\sum_{n=1}^{+\infty}\frac{C_n}{\mu_n}((-1)^n + \sin\mu_n d)\right)\right\}. \tag{15}$$

Similarly, the total heat loss from one basement wall, $Q_{wa}(t)$, is obtained as follows:

$$Q_{wa}(t) = Q_{wa,s} + Re(Q_{wa,t}\, e^{i\omega t}) \tag{16}$$

with $Q_{wa,s}$ and $Q_{wa,t}$ obtained from:

$$\tilde{Q}_{wa} = \frac{2}{c}(H_{wt} - H_{wl})\sum_{n=1}^{+\infty}\frac{D_n}{\zeta_n}\cos\zeta_n e$$

$$+\frac{2}{c}H_{wt}\sum_{n=1}^{+\infty}\frac{D_n}{\zeta_n} + \frac{2}{c}H_{wl}\sum_{n=1}^{+\infty}(-1)^n\frac{D_n}{\zeta_n}$$

$$+(H_{wt} - H_{wl})\tilde{T}_i e + H_{wl}\tilde{T}_i c. \tag{17}$$

Figure 7 shows the monthly basement floor and wall heat loss for four (4) insulation configurations:

(i) No insulation
($H_{wl} = H_{wt} = H_{fm} = H_{fe} = 10\ m^{-1}$).

(ii) Partial wall insulation
($H_{wt} = 0.5\ m^{-1}$; $H_{wl} = H_{fm} = H_{fe} = 10\ m^{-1}$; $e = 1$ m).

(iii) Full wall insulation
($H_{wt} = H_{wl} = 0.5\ m^{-1}$; $H_{fm} = H_{fe} = 10\ m^{-1}$).

(iv) Full basement insulation
($H_{wt} = H_{wl} = H_{fe} = H_{fm} = 0.5\ m^{-1}$).

In this section and Section 5, unless it is otherwise mentioned, the basement geometry, soil thermal properties, and temperatures are the same as those used in Figs. 2–6.

Figure 7(a) indicates that, during most of the year, the basement wall heat loss is reduced as a result of adding insulation on the basement envelope. The best performance is achieved when walls are fully insulated independently of the floor insulation configuration. A partially insulated wall loses more heat than an uninsulated wall during summer months but performs better during the rest of the year. This results from the strong thermal interaction between the lower part of the wall and the water table. For the uninsulated configuration and during summertime, this interaction is offset by the heat gain received by the upper part of the wall from the soil surface. Figure 7(b) indicates that the floor heat loss is significantly reduced only when insulation is placed on the entire basement envelope. Note that in the full wall insulation configuration, the floor heat loss has actually increased as a result of decreasing floor surface temperature at the edges (see Fig. 5(a)).

5. PARAMETRIC ANALYSIS

Figure 8 shows the effect of the partial wall insulation length (measured from the soil surface level) on wall annual heat flux. The annual variation of heat flux from a basement surface is characterized by three parameters: mean, amplitude, and phase lag (relative to soil surface temperature variation). As indicated in Fig. 8, as the partial insulation increases, the mean and amplitude of basement wall heat flux decreases. However, the phase lag increases from 7° (which corresponds to a time lag of 7 days) when the wall is uninsulated (i.e. $e = 0$ m) to a maximum of about 13° (i.e. a time lag of 13 days) when the insulation length is $e = 1.5$ m. The time lag decreases to 10 days as the partial wall insulation continues to increase to full basement height. This phase lag behavior occurs because of the conflicting action of both soil surface and water table on heat loss from basement walls. As longer partial insulation is placed along the basement wall, the effect of soil surface temperature on wall heat loss decreases while that of the water table increases, resulting in an increase of time lag between the wall heat flux and soil surface temperature. When the insulation is long enough to shield the lower part of the wall from the influence of the water table, the relative effect of soil temperature increases, resulting in a decrease of the wall heat flux time lag. The effect of partial wall insulation length on floor heat flux is minimal. Increasing the wall insulation length results in a very slight increase of the mean and amplitude, and in a negligible decrease of the phase lag of floor heat flux.

The effect of the U-value of the partial wall insulation of 1 m length on basement wall heat flux is illustrated in Fig. 9. As the thermal resistance of the insulation increases, that is as the H_{wl}-value decreases, the mean and amplitude of basement wall heat flux decreases, while the phase lag increases. For perfect insulation (i.e. $H_{wl} = 0\ m^{-1}$), the time lag between soil surface temperature and wall heat flux reaches a maximum value of about 18 days. The effect of the U-value of 1 m long partial wall insulation on floor heat loss is insignificant and therefore is not shown.

Figure 10 illustrates how the basement envelope heat fluxes vary with the basement depth c, when the wall is fully insulated. As shown in Fig. 10(a), the

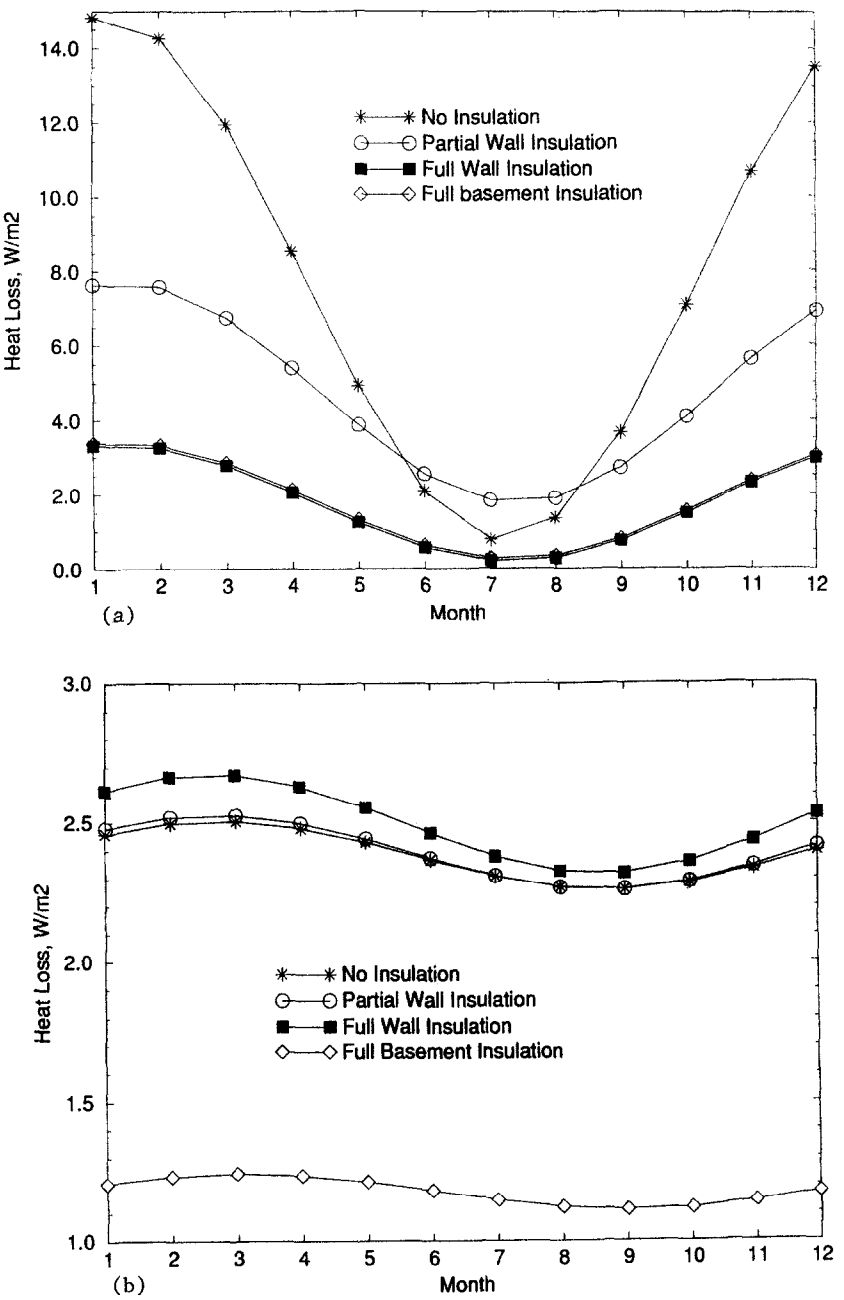

FIG. 7. Effect of insulation placement on the annual variation of (a) basement wall heat loss, (b) basement floor heat loss.

mean and amplitude of the heat loss per wall unit area are higher for shallow basements (i.e. $c < 1$ m) than for deep basements (i.e. $c > 2$ m). However, the time lag increases with depth of the basement as a result of increasing effect of the water table on wall heat flow. The basement depth affects even more significantly the heat flux from the floor. Indeed, Fig. 10(b) shows that while the mean and phase lag of the floor heat flux increases, the amplitude decreases as the basement depth increases. This behavior is the result of the assumed constant temperature water table below the basement floor. The deeper the basement is, the closer the floor is to the water table, and the stronger is the effect of the constant water table temperature on the heat flow from the basement floor.

6. SUMMARY AND DISCUSSION

A general analytical solution for steady-periodic heat transfer between partially-insulated basements and ground has been developed using the ITPE technique. Even though annual frequency was assumed

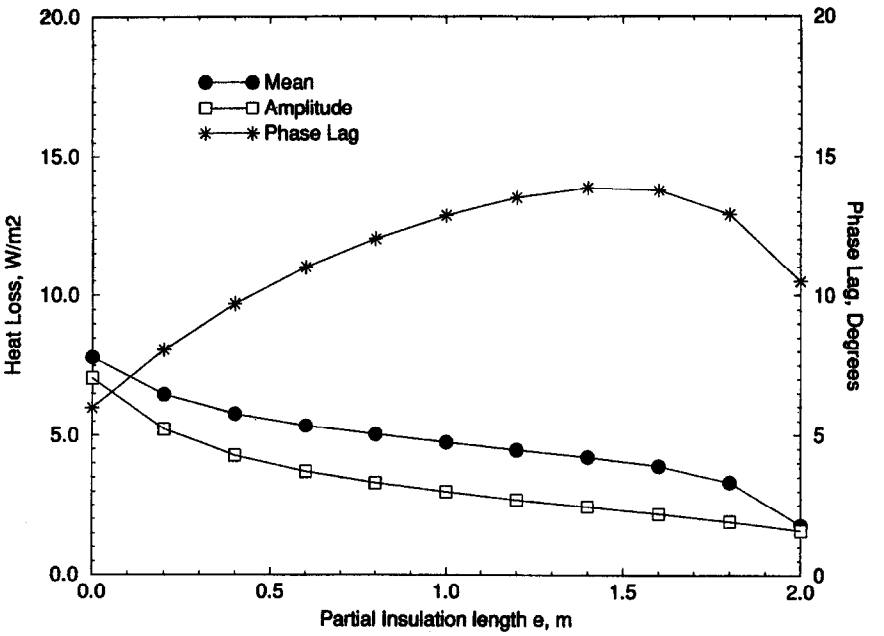

FIG. 8. Variation of the basement wall heat loss annual mean, amplitude, and phase lag as functions of the wall partial insulation length, e.

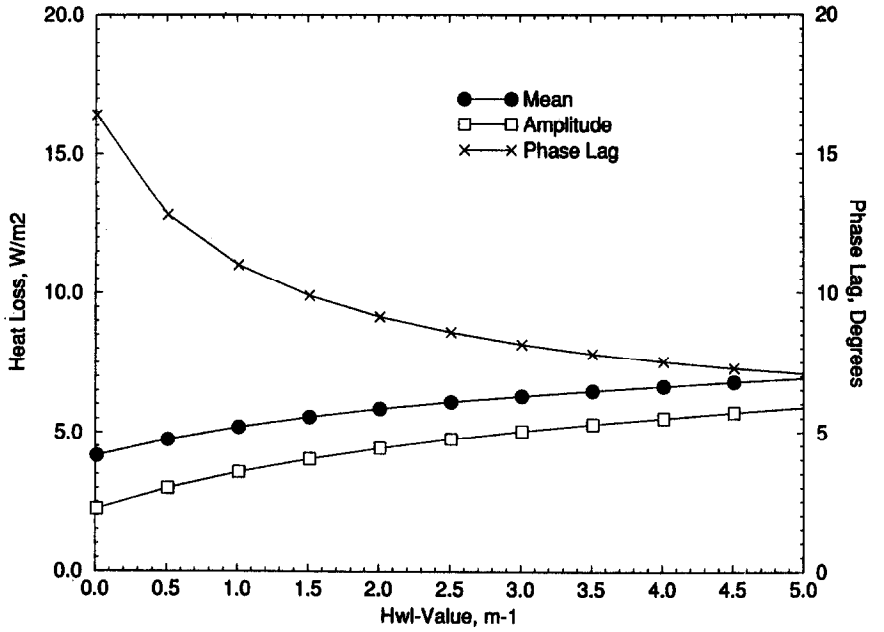

FIG. 9. Variation of the basement wall heat loss annual mean, amplitude, and phase lag as functions of the wall partial insulation H_{wl}-value.

throughout the analysis presented in the paper, the solution can be applied to any frequency. In particular, the hourly effects on foundation heat transfer of indoor temperature fluctuations can be determined using the analytical solution developed in this paper. For unheated basement or crawlspaces, the daily and seasonal indoor temperature fluctuations are significant. Thus, large errors in calculating ground heat loss would result when unconditioned foundations are modeled using a constant air temperature.

Analysis of wintertime temperature distribution within the ground has shown that wall insulation reduces the soil temperature in the vicinity of the upper wall section. This reduction in soil temperature increases the potential for foundation frost damage in very cold climates. As mentioned during the model

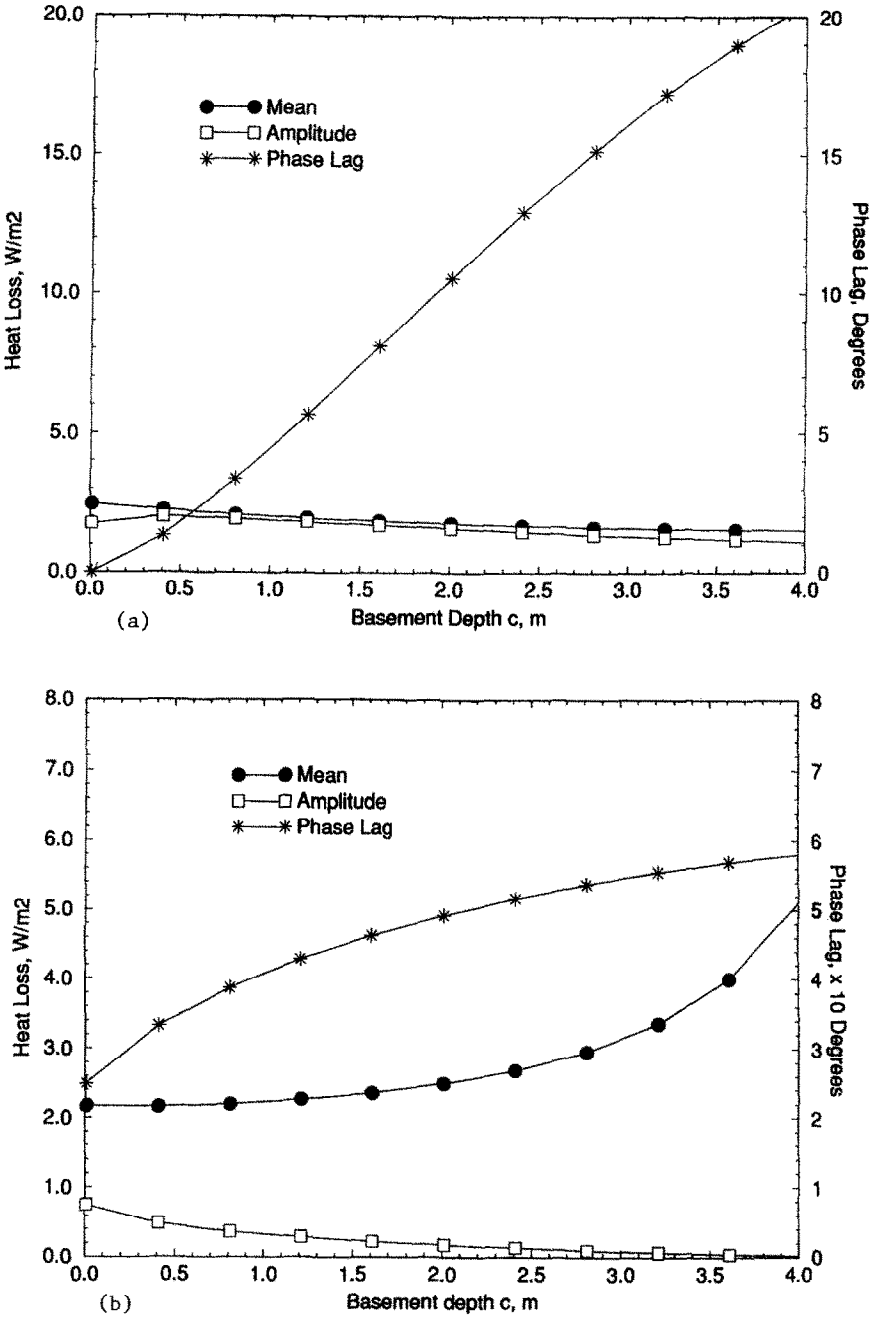

FIG. 10. Variation of the heat loss annual mean, amplitude, and phase lag as functions of the basement depth, c, for (a) basement wall, (b) basement floor.

formulation, the results obtained here apply mostly to interior insulation placements. To avoid the risk of frost-heave damage to the foundation, it is recommended to place the insulation outside the basement wall.

In addition, the analysis of both soil temperature field and monthly basement heat loss has indicated that during the summer two conflicting interactions affect the heat flow from the basement: heat gain from the soil surface and heat loss to the water table. The cooling benefits of the basement are highest when only the upper portion of the walls are insulated. However, a fully insulated basement guarantees better winter performance for both floor and walls. Thus, to properly determine the optimum basement insulation configuration, both the cooling and heating benefits should be taken into account.

Parametric study of heat loss from basement floor and walls indicated that the time lag between soil surface temperature and wall heat loss—typically on the order of few days—increases significantly with basement depth and with partial wall insulation U-

value. The same increase is obtained by increasing the partial wall insulation length as long as this length is less than 1.5 m (for a 2 m deep basement). The time lag between soil surface temperature and floor heat loss is in the order of one to two months and is mostly affected by basement depth, floor insulation U-value (and/or length), and the water table depth.

Acknowledgement—This work was supported by the American Society of Heating Refrigerating and Air Conditioning Engineers (ASHRAE)

REFERENCES

1. H. D. Bareither, N. Fleming and B. E. Alberty, Temperature and heat loss characteristics of concrete floors laid on the ground, University of Illinois Small Homes Council, Technical Report, pB93920 (1948).
2. P. H. Shipp and T. B. Broderick, Comparison of annual heating loads for various basement wall insulation strategies using transient and steady-state models. In *Thermal Insulations, Materials and Systems for Energy Conservation in the 80's*, Philadelphia, PA, American Society for Testing and Materials, ASTM-STP789, pp. 455–473, (1983).
3. R. L. Sterling and G. D. Meixel, Review of underground heat transfer research. In *Earth Sheltered Performance and Evaluation Proceedings*, Second Technical Conference (Edited by L. L. Boyer), pp. 67–74. Oklahoma State University (1981).
4. D. E. Claridge, Design methods for earth-contact heat transfer. In *Progress in Solar Energy* (Edited by K. Boer). American Solar Energy Society, Boulder, CO (1987).
5. G. P. Mitalas, Calculation of below-grade residential heat loss: low-rise residential building, *ASHRAE Trans* **93**(1), 1112–1121 (1987).
6. P. H. Shipp, Basement, crawlspace, and slab-on-grade thermal performance. In *Thermal Performance of the Exterior Envelopes of Buildings*, ASHRAE Vol. II, pp. 160–179 (1983).
7. L. S. Shen and J. W. Ramsey, A simplified thermal analysis of earth-sheltered buildings using a Fourier-series boundary method, *ASHRAE Trans.* **89**(1) 438–448 (1983).
8. L. S. Shen, J. Poliakova and Y. J. Huang, Calculation of building foundation heat loss using superposition and numerical scaling, *ASHRAE Trans.* **94**(1), 917–935 (1988).
9. K. Labs, J. Carmody, R. Sterling, L. Shen, Y. J. Huang and D. Parker, Building foundation design handbook, ORNL Report Sub/86-7214311, (1988).
10. T. Kusuda, O. Piet and J. W. Bean, Annual variation of temperature field and heat transfer under heated ground surface: slab-on-grade floor heat loss calculations, *Proc. ASHRAE/DOE Thermal Envelopes Conf.* pp. 67–94 (1982).
11. M. Krarti, D. E. Claridge and J. F. Kreider, ITPE method applications to time-varying two-dimensional ground-coupling problems, *Int. J. Heat Mass Transfer* **31**, 1899–1911 (1988).
12. M. Krarti, D. E. Claridge and J. F. Kreider, The ITPE method applied to time-varying three-dimensional ground-coupling problems, *J. Heat Transfer* **112**(4), 849–856 (1990).